A mutation of spastin is responsible for swellings and impairment of transport in a region of axon characterized by changes in microtubule composition.

Anne Couturier-Tarrade, Coralie Fassier, Sabrina Courageot, Delphine Charvin, Jérémie Vitte, Leticia Peris, Alain Thorel, Etienne Mouisel, Nuria Fonknechten, Natacha Roblot, et al.

A mutation of *spastin* is responsible for swellings and impairment of transport in a region of axon characterized by changes in microtubule composition

Anne Tarrade[1,2,†], **Coralie Fassier**[1,2,†], **Sabrina Courageot**[1,2], **Delphine Charvin**[1,2,‡], **Jérémie Vitte**[1,2], **Leticia Peris**[3], **Alain Thorel**[4], **Etienne Mouisel**[1,2], **Nuria Fonknechten**[5], **Natacha Roblot**[1,2], **Danielle Seilhean**[6], **Andrée Diérich**[7], **Jean Jacques Hauw**[6] and **Judith Melki**[1,2,*]

[1]Molecular Neurogenetics Laboratory, INSERM, U798, Evry F-91057, France, [2]Universities of Evry and Paris XI, Evry F-91025, France, [3]INSERM Unité 366-DRDC/CS CEA, Grenoble, France, [4]Centre des Matériaux, Ecole des Mines de Paris and CNRS UMR 7633, Evry, France, [5]Genoscope, Centre National de Séquençage and CNRS UMR 8030, Evry, France, [6]Assistance Publique Hôpitaux de Paris, Laboratoire de Neuropathologie Raymond Escourolle, Groupe Hospitalier Pitié-Salpétrière and Paris VI University, France and [7]Institut de Génétique et de Biologie Moléculaire et Cellulaire, INSERM, CNRS, ULP, Illkirch, France

Mutations of the *spastin* gene (*Sp*) are responsible for the most frequent autosomal dominant form of spastic paraplegia, a disease characterized by the degeneration of corticospinal tracts. We show that a deletion in the mouse *Sp* gene, generating a premature stop codon, is responsible for progressive axonal degeneration, restricted to the central nervous system, leading to a late and mild motor defect. The degenerative process is characterized by focal axonal swellings, associated with abnormal accumulation of organelles and cytoskeletal components. In culture, mutant cortical neurons showed normal viability and neurite density. However, they develop neurite swellings associated with focal impairment of retrograde transport. These defects occur near the growth cone, in a region characterized by the transition between stable microtubules rich in detyrosinated α-tubulin and dynamic microtubules composed almost exclusively of tyrosinated α-tubulin. Here, we show that the Sp mutation has a major impact on neurite maintenance and transport both *in vivo* and *in vitro*. These results highlight the link between spastin and microtubule dynamics in axons, but not in other neuronal compartments. In addition, it is the first description of a human neurodegenerative disease which involves this specialized region of the axon.

INTRODUCTION

Hereditary spastic paraplegia (HSP), or Strumpell–Lorrain syndrome, is a heterogeneous group of inherited disorders of the central nervous system, characterized by a slowly progressive bilateral spastic paraparesis. HSP may occur in either a clinically pure form or associated with other symptoms such as dementia, extrapyramidal disturbance, optic

*To whom the correspondence should be addressed at: Molecular Neurogenetics Laboratory, INSERM, University of Evry, U-798, 2 rue Gaston Crémieux, CP5724, 91057 Evry, France. Tel: +33 160874552; Fax: +33 160874550; Email: j.melki@genopole.inserm.fr
†The authors wish it to be known that, in their opinion, the first two authors should be regarded as joint First Authors.
‡Present address: Institute of Neurosciences, Swiss Federal Institute of Technology Lausanne, Ecole Polytechnique Fédérale de Lausanne, CH-1015 Lausanne, Switzerland.

neuropathy, cortical and cerebellar atrophy, peripheral neuro-pathy or seizures. The core feature of the neuropathology is pallor of the lateral corticospinal tracts. The dorsal columns are also involved, particularly the fasciculus gracilis. The spinal cerebellar tracts are variably affected. Loss of the Betz cells of the motor cortex has occasionally been reported, but motor neurons of anterior horns are generally spared. The consistently distal pattern of involvement of the corticospinal tracts and dorsal columns has led to the suggestion that the pathology of HSP represents a dying back axonopathy.

HSP shows considerable genetic heterogeneity and can be inherited as an autosomal dominant (AD-HSP), autosomal recessive or X-linked recessive disorder (reviewed in 1). Genes identified to date include *spastin*, *spartin*, *kinesin heavy chain* (*KIF5A*), *heat shock protein 60* (*HSP60*), *atlastin*, *paraplegin*, *L1 cell adhesion molecule* (*L1-CAM*), *proteolipid protein* (*PLP*), *NIP1A*, *Maspardin*, *BSCL2*, *ZFYVE27* and *REEP1* (reviewed in 2). The identification of genes respon-sible for HSP highlighted the diversity of molecular defects underlying HSP, including impairment of mitochondrial func-tion (paraplegin and HSP60), failure of axonal transport (kinesin heavy chain) or impairment of axoglial interaction (L1-CAM and PLP).

The most prevalent form of AD-HSP (40%) is linked to the SPG4 locus on chromosome 2p21, which encodes a novel protein named spastin (3). Mutation analysis of the SPG4 locus has previously shown various DNA alterations of the *spastin* gene including nonsense (15%), deletion (23%), inser-tions (7.5%), splice site mutations (26.5%) or missense mutations (28%; 4–10). It is likely that nonsense or splice site mutations result in loss of function (11). However, some *spastin* missense mutations could act as dominant negative mutations (12). The *spastin* gene is ubiquitously expressed and encodes a protein of 616 amino acids. Its C-terminus shows significant homology to members of the AAA protein family (ATPase associated with diverse cellular activities, residues 376–505, 3 and 13). AAA proteins are involved in a wide variety of functions including metalloprotease activity, involvement in vesicle and organelle biogenesis, cell cycle regulation, ribosome assembly in mitochondria or as components of the 26S proteasome (13). The AAA ATPase domain of spastin is homologous to katanin, a microtubule-severing protein, suggesting a similar function for spastin. In neurons, katanin appears to be a source of non-centrosomal microtubules (14). Katanin overexpression in cultured mammalian neurons alters process outgrowth (15), and overexpression in *D. Melanogaster* results in developmental abnormalities of the mushroom body (16). Interestingly, Errico *et al*. (17). suggested a role for spastin in microtubule dynamics *in vitro*. Wild-type spastin proteins, transfected into neuronal and non-neuronal cells, interacted transiently with microtubules, resulting in the disassembly of the micro-tubules. This supports a role for spastin in microtubule sever-ing. It is now clear that spastin is sufficient for microtubule severing and several disease-associated mutations in spastin abolish both ATPase and severing activities (18). In addition, spastin contains a microtubule interacting and organelle trans-port domain (MIT, residues 114–191) sharing homology with spartin. Spartin mutations cause another inherited spastic para-plegia associated with mental retardation (19). Other functions

of spastin have been suggested from the identification of spas-tin's partners using a variety of approaches. These include the centrosomal protein NA14, CHMP1B, atlastin, Reticulon1 and ZFYVE27, which are proteins involved in membrane traffic events; however, these interactions remained to be confirmed *in vivo* (17,20–23).

In order to elucidate the pathogenesis of HSP linked to *spastin* mutation, loss-of-function models have been used. When drosophila *Dspastin* was deleted, aberrantly stabilized microtubule cytoskeleton in neurons was observed and defects in synaptic growth and neurotransmission were also detected (24). Recently, knock-down spastin function in zebra-fish embryos resulted in dramatic defects in motor axon growth during development (25).

HSP linked to *spastin* mutations affects mainly corti-cospinal tracts without any involvement of the peripheral nervous system. Therefore, the generation of an animal model in higher organisms should contribute to refine the HSP pathogenesis. To this end, we have generated mice carry-ing a deletion of the *Sp* gene resulting in a frameshift and the lack of the AAA domain through homologous recombination. This mutation mimicks nonsense or frameshift mutations of human Sp exon 5, which are found in 15% of HSP patients and result in the absence of the AAA cassette (4). Mutant mice develop a progressive axonopathy characterized by focal swellings of axons without any loss of neurons. In addition, marked accumulation of organelles and intermediate filaments was observed within axonal swellings. Primary cul-tures of cortical neurons derived from mutant embryos showed normal viability and neurite outgrowth. However, they display neurite swellings associated with an impaired retrograde trans-port of organelles. These defects occur in a specialized region of the neurite close to, but distinct from, the growth cone. This region is characterized by the transition between a stable microtubule domain rich in detyrosinated α-tubulin and a dynamic one, composed almost exclusively of tyrosinated α-tubulin. Our data highlight the link of spastin to microtubule dynamics in axons, but not in other cell compartments.

RESULTS

Generation of mice carrying a heterozygous or homozygous intragenic deletion of the *spastin* gene leading to the lack of the AAA domain

To generate a mouse model of HSP, we used gene targeting in murine embryonic stem cells to introduce a truncating mutation into the *spastin* (*Sp*) gene through homologous recombination. Because we wanted the mice to survive, we used a targeting vector that includes loxP sequences in introns 4 and 7. In intron 4, the *NeoR* gene was introduced at the 3′ end of the loxP sequence (Fig. 1A). Southern blot analysis of embryonic stem cells confirmed homologous recombination at the Sp locus (Fig. 1B). Mice heterozygous or homozygous for the loxP-flanked Sp allele (*Sp^F*) appear similar in size and morphology to wild-type mice. No alterna-tive splicing of Sp exons or variation in transcript amount was detected by RT–PCR amplification analysis of RNA extracted from various tissues of the (*Sp^{F/F}*) or (*Sp^{F/+}*) mice, indicating that neither the *NeoR* gene nor the loxP sequences
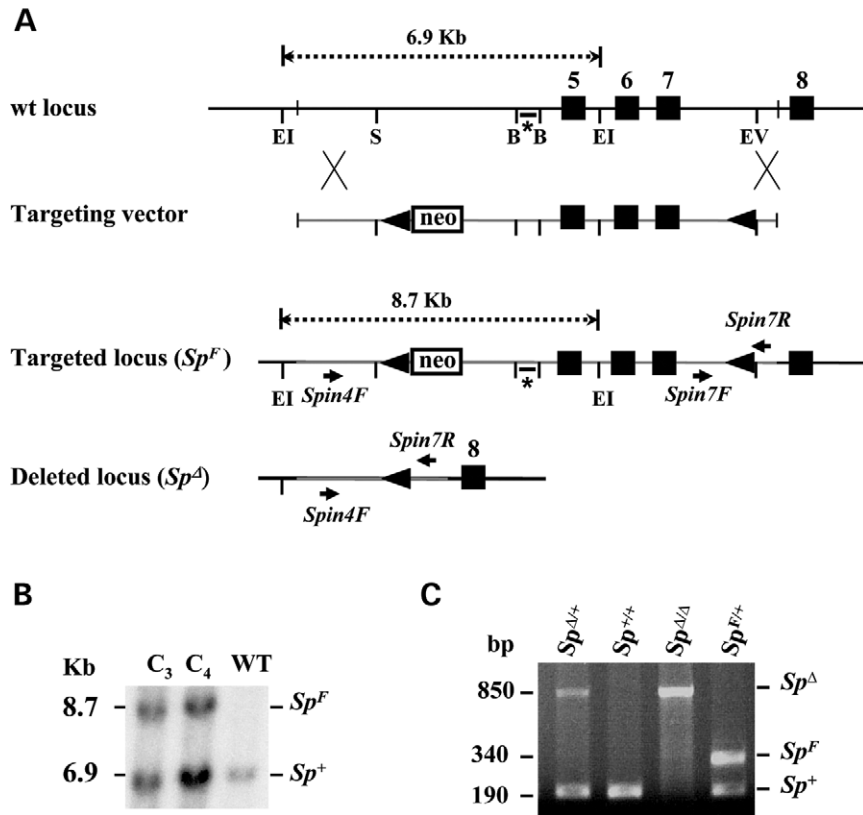
Figure 1. Mutagenesis of the murine *spastin* gene. (**A**) The panel shows the wild-type genomic *spastin* locus (wt), the targeting vector, the targeted locus (Sp^F) and the Cre-mediated deleted locus (Sp^Δ). Filled rectangles indicate exons and arrowheads indicate the position of loxP sequences. The locations of the PCR primers used to screen for the presence of targeted and deleted locus are shown. The DNA probe (indicated by asterisk) used to confirm the homologous recombination is also given. (**B**) Southern blot analysis of DNA from wild-type ($Sp^{+/+}$) and ($Sp^{F/+}$) ES cells. Digestion of DNA with *Eco*RI (EI) generates a 6.9 kb wild-type and 8.7 kb 'floxed' fragments ($Sp^{F/+}$) which are detected with a probe derived from *Sp* intron 4 (asterisk). (**C**) PCR amplification of the (Sp^+), (Sp^F) and (Sp^Δ) alleles from DNA of ($Sp^{+/+}$), ($Sp^{F/+}$), ($Sp^{\Delta/+}$) and ($Sp^{\Delta/\Delta}$) mice using *Spin4F*, *Spin7F* and *Spin7R* primers. EI, *Eco*RI; B, *Bam*HI; EV, *Eco*RV; S, *Sph*1; Neo, neomycine resistance cassette gene.

have a deleterious effect on *spastin* RNA splicing or transcription (data not shown). Mice heterozygous for the Sp^F allele were crossed to transgenic mice expressing the *Cre* recombinase transgene under the control of the *CMV* promoter (26). Cre recombinase expression in the germline led to the generation of mice carrying a heterozygous deletion of *spastin* exons 5–7 ($Sp^{\Delta/+}$). ($Sp^{\Delta/+}$) mice gained weight normally after birth and were fertile. They were maintained on a C57BL6/J genetic background and then intercrossed. Progeny carrying a heterozygous ($Sp^{\Delta/+}$) or homozygous ($Sp^{\Delta/\Delta}$) deletion of *Sp* exons 5–7 in all cell types (Fig. 1C) were observed, with the expected ratio for each genotype (50 and 25%, respectively). ($Sp^{\Delta/\Delta}$) mice have a normal life expectancy but were sterile. Truncated *Sp* transcripts lacking exons 5–7 were detected in various tissues including brain (Fig. 2A) and confirmed by sequence analysis of PCR amplification products of reverse transcripts (Fig. 2B). Alternative spliced products linking exons 4–8 were observed, leading, as expected, to a frameshift and a stop codon 29 bp after the exons 4–8 junction (Fig. 2B). This mutated protein lacks the AAA cassette. Using rabbit polyclonal antibodies (4828), which recognize an epitope of spastin located within the deleted region, immunoblot analysis revealed the full-length 60 kDa spastin in wild-type, but not ($Sp^{\Delta/\Delta}$) mice (Fig. 2C).

Heterozygous or homozygous deletion of *spastin* exons 5–7 results in progressive axonopathy of the central nervous system

Semi-thin sections of the brain and spinal cord of 12-month-old mutant mice ($Sp^{\Delta/\Delta}$) did not reveal either disorganization or developmental defects of the CNS (Online Supplementary Material 1). We asked whether the degeneration of the spinal tracts, which occurs in the human disease, also occurs in mutant mice. Transverse semi-thin sections of spinal cord were examined in 4- and 12-month-old ($Sp^{\Delta/\Delta}$) mutant and ($Sp^{F/+}$) or ($Sp^{+/+}$) control mice using toluidine blue staining (three mice in each group). The organization of descending and ascending tracts was normal. In 4-month-old mutant mice ($Sp^{\Delta/\Delta}$), the striking feature was the presence of axonal swellings in the white matter of the spinal cord of mutant mice (1 ± 0.5 and 4 ± 0.5 SE axonal swellings per spinal cord section at the lumbar and cervical level, respectively; Fig. 3). We quantified the number of axonal swellings in 12-month-old mutant mice ($n = 3$) and
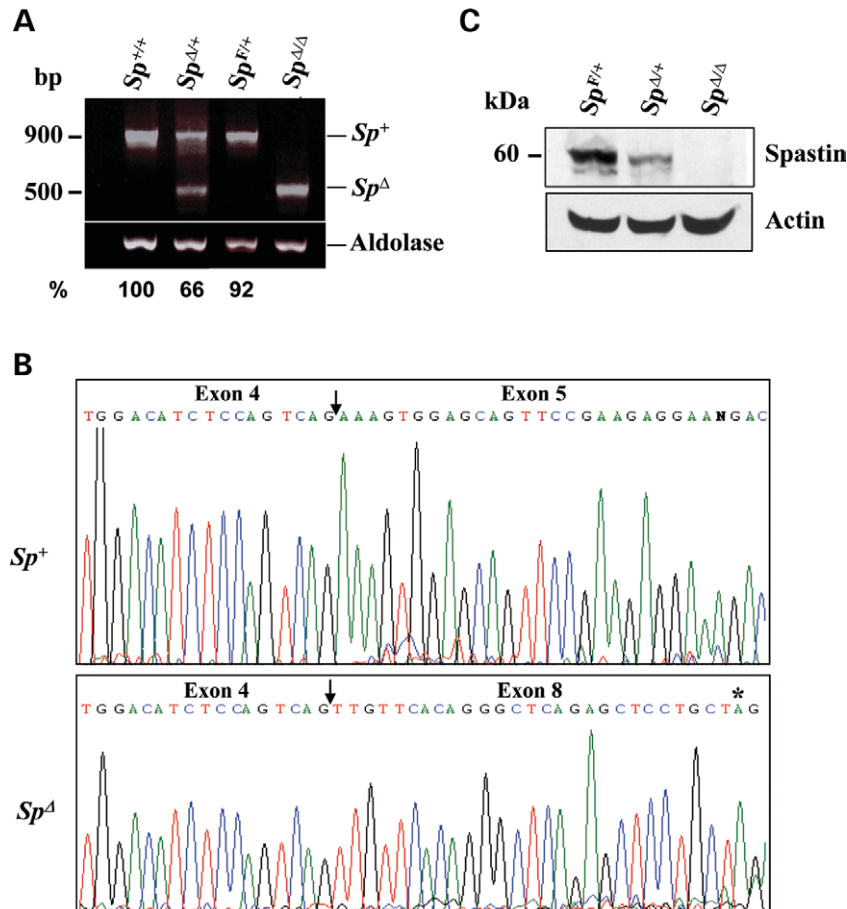
Figure 2. Analysis of *spastin* transcript and protein in control and mutant mice. (**A**) Transcript analysis of *Sp* from the brain of 2-month-old mice. RT–PCR amplification of *Sp* was performed from total RNA using primers *Slymph* and *ex12spas*. RT–PCR amplification reveals the *Sp* transcripts retaining (900 bp) or lacking exons 5–7 (500 bp). The abundance of full-length transcripts (Sp^+) was evaluated by densitometric analysis of *spastin* and *aldolase* PCR products. The ratio of spastin to aldolase expression was calculated, and then the relative amount of *spastin* in ($Sp^{F/+}$) and ($Sp^{\Delta/+}$) tissues was expressed as a percent of wild-type *spastin* level ($Sp^{+/+}$). (**B**) Sequence analysis of the RT–PCR products generated from the RNA of ($Sp^{+/+}$) and ($Sp^{\Delta/\Delta}$) mice. Arrows indicate the boundaries of each exon and an asterisk shows the stop codon in exon 8. (**C**) Using rabbit polyclonal antibodies (4828), immunoblot analysis of spastin shows the full-length 60 kDa spastin in brain of ($Sp^{F/+}$) but not ($Sp^{\Delta/\Delta}$) mice. Note the half dose of spastin in ($Sp^{\Delta/+}$) mice. Actin was used as internal control.

found an increased number of axonal swellings with age, which was more pronounced in the lumbar (7.3 ± 1.7 SE, 7-fold increase, $P = 0.02$) than in the cervical levels (8 ± 1.5 SE, 2-fold increase; Fig. 3F). Axonal swellings were observed in both descending and ascending tracts of the spinal cord. No axonal swellings were observed in control ($Sp^{F/+}$) or ($Sp^{+/+}$) mice at either 4 or 12 months of age ($n = 3$ in each group). In 24-month-old mutant mice, numerous swelling axons with thin myelin sheaths were observed, with dramatic disorganization of cytoskeletal components in corticospinal tracts (Fig. 4H). These results show a progressive axonal defect in mutant mice. To determine the extent of axonal swellings, longitudinal semi-thin sections of spinal cord were examined and axonal swellings were found to be limited in length (Fig. 3E). In contrast, no change was detected in the density or morphology of motor neuron cell bodies, in either the motor cortex or spinal cord of 12- or 24-month-old homozygous mutant, when compared with control mice (Online Supplementary Material 2). In addition, no increased proportion of glial cells was observed in either

the motor cortex or spinal cord of mutant mice (data not shown). These results indicate that the spastin mutation results in a defect which is restricted to axons. To determine whether this defect involves the peripheral nervous system, transverse semi-thin sections of sciatic nerves were examined in 12-month-old ($Sp^{\Delta/\Delta}$, $n = 3$) mutant and ($Sp^{F/+}$, $n = 3$) control mice. No axonal swelling was observed in the sciatic nerve of 12-month-old mutant mice (Online Supplementary Material 2) or in older mice (24 months of age, data not shown), indicating that the axonal defect was restricted to the central nervous system of mutant mice, similar to what is found in human HSP linked to *spastin* mutations.

To determine whether the occurrence, or the number, of axonal swellings correlated with a dose effect of wild-type *spastin* allele, semi-thin sections of spinal cord from 12-month-old ($Sp^{\Delta/+}$) heterozygous mutant mice were analysed ($n = 3$). Axonal swellings were observed in heterozygous mice in both cervical and lumbar spinal tracts. At the lumbar level of the spinal cord, the number of axonal swellings was markedly lower in 12-month-old heterozygous
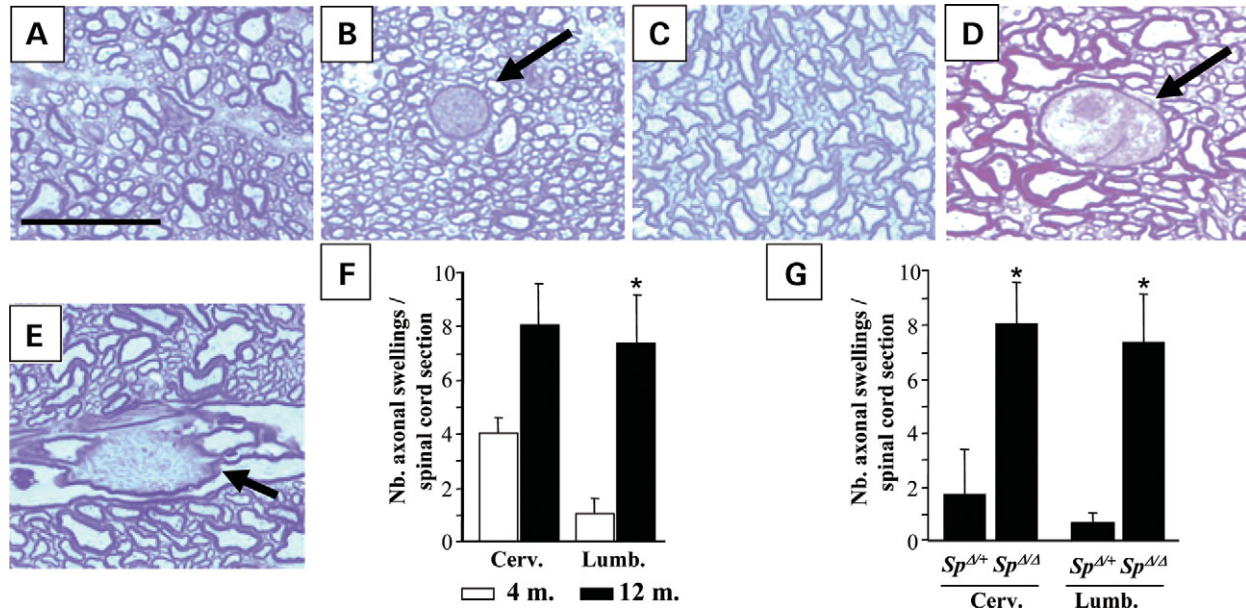
Figure 3. Axonal swellings in spinal cord of mutant mice. (**A–E**) Toluidine blue staining of transverse (A–D) and longitudinal (E) semi-thin sections of spinal cord from control ($Sp^{F/+}$) (A and C) and mutant ($Sp^{\Delta/\Delta}$) (B, D and E) mice of 4- (A and B) and 12 months of age (C–E). Arrows show the axonal swellings on transverse (B and D) or longitudinal sections (E). Scale bar: 20 μm (A–E). (**F** and **G**) Number of axonal swellings per spinal cord section. Asterisks indicate statistically significant higher number of axonal swellings ($P < 0.05$) in 12-month-old when compared with 4-month-old mutant mice ($Sp^{\Delta/\Delta}$) (F) and in 12-month-old homozygous ($Sp^{\Delta/\Delta}$) when compared with heterozygous ($Sp^{\Delta/+}$) mutant mice (G). Cerv, cervical; Lumb, lumbar; m, month. Vertical bars indicate standard error.

(0.7 ± 0.3 SE, $n = 3$) compared with homozygous mutant mice (7.3 ± 1.7 SE, $n = 3$, 11-fold decrease, $P = 0.02$; Fig. 3G). Swellings were less frequent in the cervical spinal cord of heterozygous mutant mice when compared with homozygous mice (Fig. 3G). These data strongly suggest a dose effect of wild-type spastin on the severity of the axonal defect.

The surfaces of non-swollen axons were then evaluated in the corticospinal tract of 12-month-old mutant ($Sp^{\Delta/\Delta}$, $n = 3$) and compared with control mice ($Sp^{F/+}$, $n = 3$) to determine whether the axonal swellings reflected a generalized axonal defect. At least 450 axons were analysed in each mouse. Interestingly, no difference was detected, suggesting that the axonal swellings occur in specific regions of axons (Online Supplementary Material 3).

Swollen axons contain an abnormal accumulation of organelles and cytoskeletal components

To examine the content of axonal swellings, thin sections of the spinal cords of 12-month-old homozygous mutant and control mice were processed for electron microscopy. Swollen axons, surrounded by a thin myelin sheath, contained a large number of organelles including mitochondria, lysosomes and peroxysomes, associated with multilamellar dense bodies and vacuoles (Fig. 4). In addition, abnormal accumulation and disorganization of neurofilaments were observed. In older mutant mice (24 months of age), marked depletion of cytoskeletal components, including microtubules, was noted in the axonal swellings (Fig. 4H).

To determine whether the abnormal accumulation of organelles was widespread in neuronal compartments, semi-thin sections of motor cortex and anterior horns of the spinal cord of 12-month-old homozygous mutant mice ($n = 3$) and control ($n = 3$) were examined. Neither accumulation of organelles nor aggregates in the cytoplasm or nuclei of motor neuron cell bodies were detected (Online Supplementary Material 2).

These data indicated that the *spastin* mutation is responsible for a progressive axonopathy, characterized by focal axonal swellings associated with an accumulation of organelles, suggesting an impairment of axonal transport. We then went on to quantify the level of motor proteins involved in this process, including dynein intermediate chain, p150 and p50 dynactin, kinesin light chain together with cytoskeletal components including actin, neurofilament subunits and tyrosinated (Tyr) and detyrosinated (Glu) tubulins. Brain and spinal cord extracts of 12- or 24-month-old homozygous mutant and control mice were analysed by western blotting. No difference in the amount of proteins was observed (Online Supplementary Material 4; data not shown). These data indicate that the defect of axonal transport, as suggested by the massive accumulation of organelles, was not associated with any obvious quantitative changes in motor proteins or in cytoskeletal components. It was not unexpected, considering the focal distribution and low frequency of axonal swellings in mutant mice.

Motor function of *spastin* mutant mice

To determine whether mutant mice had impaired motor function, gait parameters were evaluated by footprint analysis of 4-, 12- and 22-month-old control ($Sp^{F/+}$) and homozygous
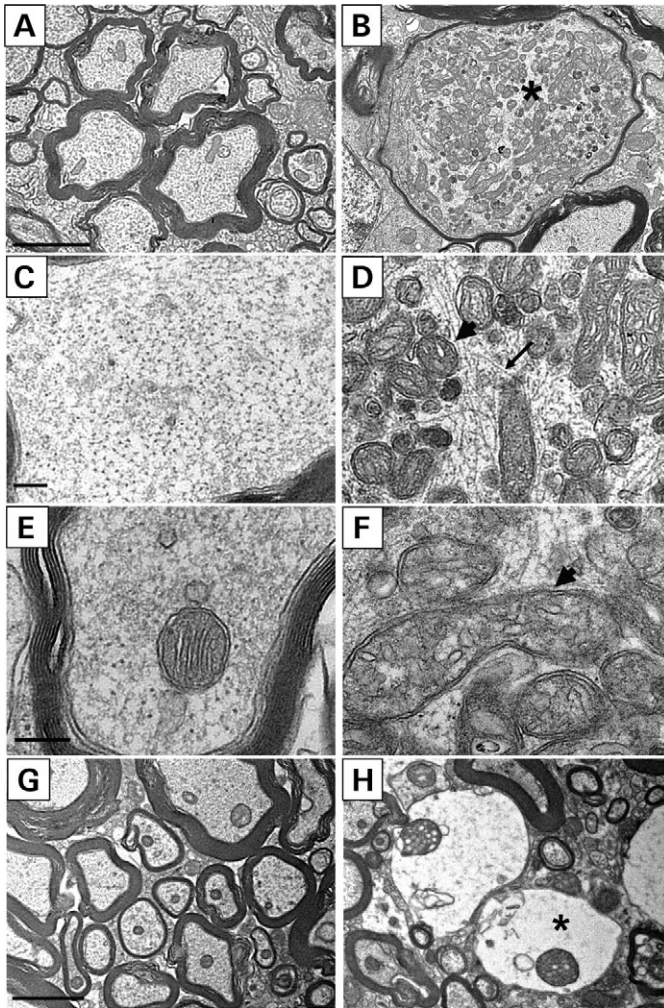
Figure 4. Ultrastructural analysis of axonal swellings in the spinal cord of mutant mice. Ultrathin sections of lumbar spinal cord of 12-month-old control ($Sp^{F/+}$) (**A**, **C** and **E**) and mutant mice ($Sp^{\Delta/\Delta}$) (**B**, **D** and **F**). Note the axonal swelling (B) (asterisk) filled with organelles (D and F) (arrowheads) and filaments (D) (arrow) in mutant spinal cord (B, D and F). In 24-month-old mutant mice (**H**), dramatic disorganization of the axoplasm was observed in swellings (asterisk) when compared with control of the same age (**G**). At each age, three control and mutant mice were analysed. Scale bar: 2 μm (A, B, G and H); 0.2 μm (C–F).

mutant mice ($Sp^{\Delta/\Delta}$). The alternation coefficient, describing the uniformity of step alternation and step length, revealed a defect in both parameters in 22-month-old mutant mice when compared with control (Fig. 5A). In addition, examination of the critical speed (CS) (27), which reflects aerobic motor capacity, showed a 35% decrease of the CS in mutant mice from 15 to 24 months of age compared with 17% in control mice ($P = 0.04$, Fig. 5B). In contrast, evaluation of the spontaneous motor activity demonstrated a frequency of slow and fast movements or rearing (vertical activity), which was similar in homozygous mutant and control mice (Fig. 5C). These data indicate that axonal degeneration of the CNS results in a late and moderate motor defect.

The *Spastin* mutation phenotypically gives rise to swellings and impairment of retrograde transport in a specialized region of the axon in primary cultures

We cultured ($Sp^{\Delta/\Delta}$), ($Sp^{\Delta/+}$) and ($Sp^{+/+}$) cortical neurons in order to examine the neuronal phenotype *in vitro*. Cortical neurons were collected from 14.5 days post-coitum embryos (d.p.c.), plated and observed for six successive days. The viability of cells was not affected by the Sp^{Δ} mutation, as defined by the number of ($Sp^{\Delta/\Delta}$) mutant and ($Sp^{+/+}$) control neuronal cells present 6 days after plating (Fig. 6A). In addition, vital (trypan blue dye) or TUNEL staining did not reveal any differences between ($Sp^{+/+}$) control and mutant neurons ($Sp^{\Delta/\Delta}$) (data not shown). Immunolabelling of phosphorylated heavy subunit neurofilament or acetylated tubulin revealed that the cortical neurons develop neurites upon differentiation. Six days after plating, immunolabelling of neurofilaments, the intermediate filament specific to neurons, was observed in >99% of cells, indicating that neuronal cells were not contaminated by glial or other non-neuronal cell types. Consistent with this result, immunolabelling with glial fibrillary acidic protein (GFAP), which is a marker specific to astrocytes, never revealed any positive cells (data not shown). The density of neurites was evaluated in control ($Sp^{+/+}$) and heterozygous ($Sp^{\Delta/+}$) and homozygous mutant cells ($Sp^{\Delta/\Delta}$), 1 or 6 days after cell plating. No difference in neurite density was detected between mutant and control cells (Fig. 6B and C).

Although the immunolabelling of neurofilament or acetylated tubulin did not reveal any neurite defect 1 day after plating, mutant cells did, however, develop neurite swellings from day 4. They were characterized by focal swellings located exclusively in distal regions of the neurites (Fig. 7). They were not associated with neurite branching and were close to, but distinct from, the growth cone, as determined by immunolabelling of acetylated tubulin and actin (Fig. 8). Six days after plating, the number of neurite swellings was measured on acetylated tubulin immunolabelled neurons relative to 100 DAPI-stained nuclei. At least 1000 neurons per embryo were analysed in control ($Sp^{+/+}$, $n = 3$) heterozygous ($Sp^{\Delta/+}$, $n = 4$) and homozygous ($Sp^{\Delta/\Delta}$, $n = 3$) mutant cells. A mean of 3.86 ± 0.001, 0.7 ± 0.001 and $0.08 \pm 0.003\%$ neurite swellings were observed in ($Sp^{\Delta/\Delta}$), ($Sp^{\Delta/+}$) and ($Sp^{+/+}$) cells, respectively (Figs 6D and 7). Similar results were observed using a neurofilament specific antibody (data not shown). These data demonstrate that ($Sp^{\Delta/\Delta}$) neurons exhibit a marked increased frequency of neurite swellings compared with heterozygous ($Sp^{\Delta/+}$) or wild-type cells ($Sp^{+/+}$, $P < 0.001$ for each comparison), in agreement with *in vivo* data. In addition, the data show that a half dose of spastin is sufficient to attenuate the cellular phenotype, suggesting a loss of function of the mutated spastin. To further investigate this hypothesis, transfection experiments of mutated *spastin* fused to GFP (*GFP-Sp$^{\Delta}$*) or GFP alone were performed on primary cultures of wild-type cortical neurons ($Sp^{+/+}$). No neurite swellings were observed in 1100 GFP-Sp$^{\Delta}$ positive neurons (Fig. 7). These data indicate that overexpression of this mutation did not have a dominant effect.

Interestingly, phase contrast analysis of neurite swellings revealed an increased density of axoplasm in the proximal
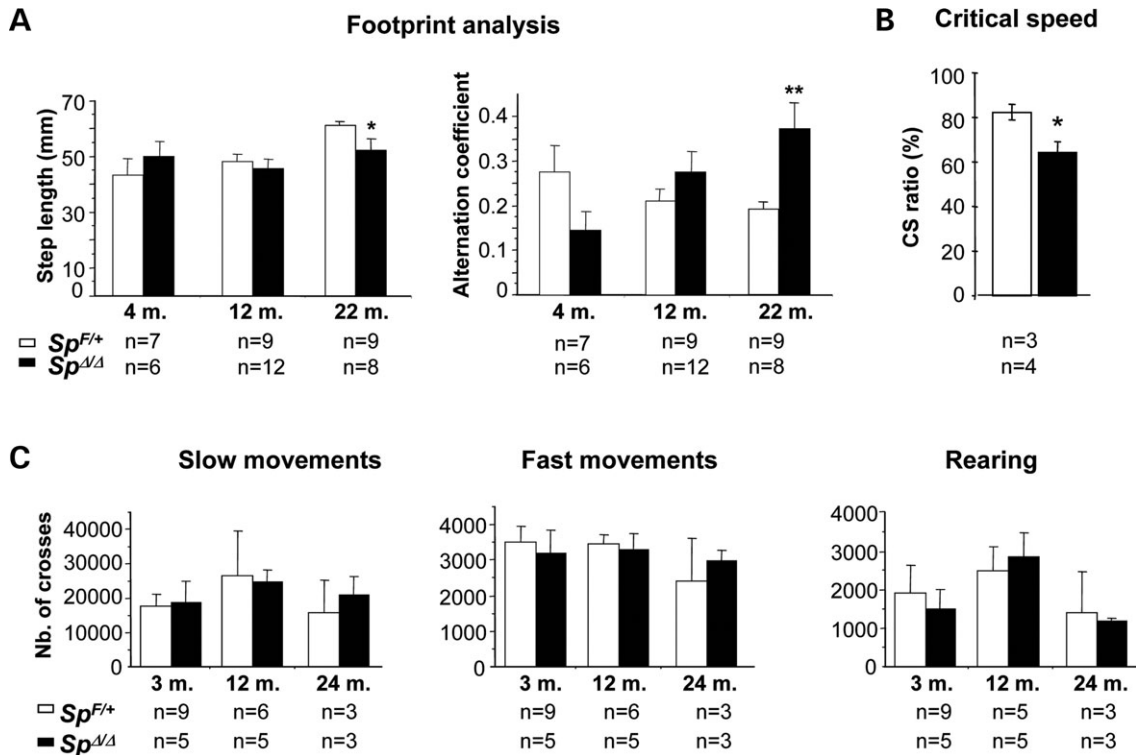
Figure 5. Analysis of motor behaviour. (**A**) Footprint analysis of 4-, 12- and 22-month-old control ($Sp^{F/+}$) and mutant mice ($Sp^{\Delta/\Delta}$). The progression of the step length and alternation coefficient is presented. Motor defect was detected in 22-month-old homozygous mutant mice when compared with control mice. (**B**) CS was examined in 15- and 24-month-old control ($Sp^{F/+}$) and mutant mice ($Sp^{\Delta/\Delta}$). The results are presented as the ratio of the CS at 24 months to that at 15 months of age. A 35% decrease in the CS was observed in mutant mice from 15 to 24 months of age. (**C**) Spontaneous motor activity. Slow, fast movements and rearings were evaluated in 3-, 12- and 24-month-old ($Sp^{F/+}$) and ($Sp^{\Delta/\Delta}$) mice. The number of animals of each group is indicated below each graphic. Vertical bars indicate standard error. Asterisks indicate P-value <0.05 (*) or <0.01 (**).

part of the swellings (Figs 8B and 9A). To determine whether this might reflect an impairment of axonal transport, mitochondria and peroxysome labelling was performed using Mitotraker and anti-catalase antibody, respectively (Fig. 9). Surprisingly, abnormal accumulation of both organelles was observed in the proximal part of neurite swellings. In addition, abnormal accumulation of peroxysomes was shown in the growth cones downstream from swellings, further suggesting a defect in retrograde axonal transport (Fig. 9). These organelles did not accumulate in other cell compartments. The results strongly suggest a focal impairment of retrograde transport of organelles in mutant neurons.

Neurite swellings occur in the distal region of the axon that differs in composition and stability of microtubules

Surprisingly, neurite swellings were exclusively localized in close proximity to, but distinct from, the growth cone (Figs 7–9). The distance between the terminal portion of neurite swellings and the end of the neurite, as determined by immunolabelling of acetylated tubulin, was 20–100 μm. Swellings were never associated with neurite branching. Axons consist of stable and labile microtubule domains that are distinguishable on the basis of their α-tubulin composition: labile microtubules are rich in tyrosinated α-tubulin (Tyr), whereas stable microtubules are rich in α-tubulin that has

been post-translationally detyrosinated and/or acetylated (Glu) (28,29). In the distal region of the axon, contiguous with the growth cone, there is an abrupt transition between a proximal domain rich in stable microtubules (Glu-tubulin) and a more distal domain almost exclusively composed of dynamic microtubules (Tyr-tubulin). To determine whether neurite swellings occurred closed to this transition, immunolabelling of Tyr- and Glu-tubulins was performed in control and mutant neurons in culture (Fig. 10). In the control, the most distal part of the axon stained brightly for Tyr-tubulin. The intensity of staining then gradually decreased, reaching a constant level over the remaining portion of the axon. The same control axons stained uniformly for Glu-tubulin all along their length, except in the distal part of axons in which a dramatic decrease or no staining was observed (Fig. 10). In mutant neurons, the transition between stable and dynamic microtubules was also observed. In addition, no difference in Tyr- or Glu-tubulin expression levels was observed between control and mutant neurons (Online Supplementary Material 4). In contrast, all neurite swellings were strikingly localized proximal to the transition between stable and dynamic microtubules (Fig. 10). Microtubules in the axonal swelling were predominantly Glu, suggesting an additional stabilization in this region. In contrast, microtubules in the distal part of the axon, immediately after the swelling, were mainly composed of Tyr-tubulin, indicating the dynamic property of
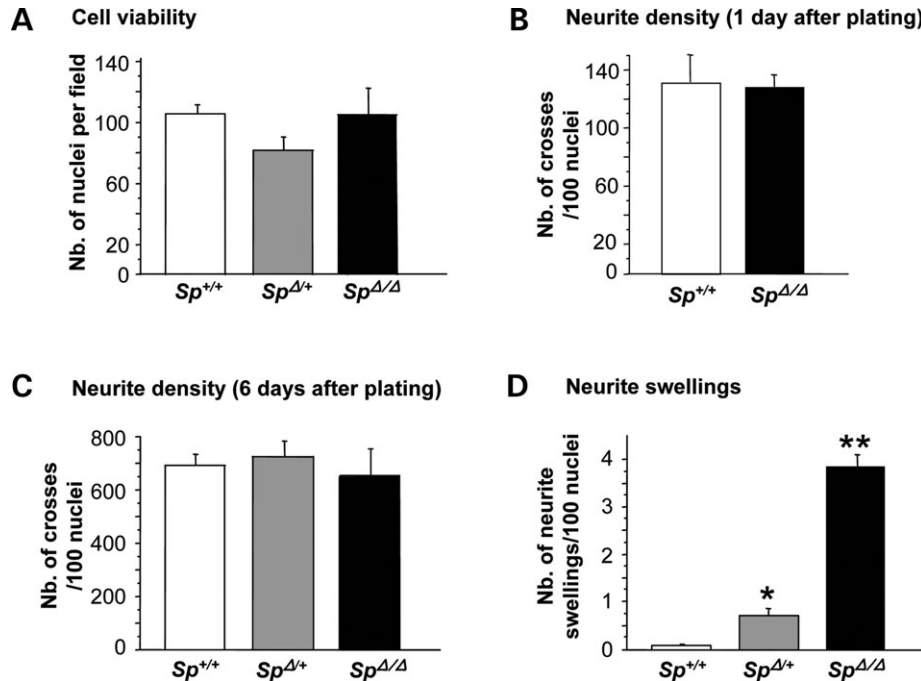
Figure 6. Characteristics of cultured cortical neurons carrying a *spastin* mutation. (**A**) Cell viability was estimated from the mean number of nuclei per field 6 days after plating of primary cultures of cortical neurons. Wild-type ($Sp^{+/+}$) ($n = 3$), heterozygous ($Sp^{\Delta/+}$) ($n = 4$) and homozygous mutant embryos ($Sp^{\Delta/\Delta}$) ($n = 3$) were analysed. At least 10 fields were analysed per embryo. (**B** and **C**) Neurite density was examined 1 (B) and 6 days (C) after plating of cortical neurons from wild-type ($Sp^{+/+}$) ($n = 3$), heterozygous ($Sp^{\Delta/+}$) ($n = 3$) and homozygous mutant embryos ($Sp^{\Delta/\Delta}$) ($n = 3$). At least 180 nuclei were analysed per embryo. (**D**) Frequency of neurite swellings was evaluated in primary cultures of cortical neurons 6 days after plating. Neurons were derived from wild-type ($Sp^{+/+}$) ($n = 3$), heterozygous ($Sp^{\Delta/+}$) ($n = 4$) and homozygous mutant embryos ($Sp^{\Delta/\Delta}$) ($n = 3$). The number of neurite swellings was much higher in homozygous than in heterozygous or wild-type cells. Asterisks indicate statistically different numbers of neurite defects between heterozygous and wild-type cells (*$P < 0.02$) or between homozygous and heterozygous mutant or wild-type cells (**$P < 0.001$). At least 1000 neurons were analysed per embryo. Vertical bars indicate standard error.

those polymers. No detectable defect was observed in other cell compartments. These results indicate that the focal swellings associated with an impaired retrograde transport of organelles occur in a specialized region of the axon which is characterized by a rapid transition between a stable and dynamic microtubule network (28,29).

DISCUSSION

In this study, we generated mice carrying a deletion of the *spastin* gene leading to a premature stop codon, thereby mimicking 15% of the Sp mutations found in HSP patients. This mutation is responsible for focal axonal swellings associated with marked accumulations of organelles and intermediate filaments, which suggest an impairment of axonal transport *in vivo*. The axonopathy is restricted to the central nervous system. An increased frequency of axonal defects as well as disorganization of cytoskeletal components in swollen axons is observed with age.

In addition, focal axonal swellings were observed in both descending and ascending tracts of the spinal cord, suggesting that the defect is not restricted to the corticospinal tract. These results, associated with the absence of a developmental defect of the central nervous system, indicate that mutated *spastin* is responsible for the degenerative process. Importantly, no loss of motor neurons was observed even at the latest stage

(24 months of age), indicating that *Sp* mutations lead exclusively to axonal disease. The mutation causes late and moderate motor defect in mice, indicating that the axonal degenerative process is slowly progressive, in agreement with the late occurrence of symptoms in adult HSP patients and the mild course of the disease.

Trotta *et al*. (24) have shown that loss of *Dspastin* results in the accumulation of stabilized tubulin and defects in synaptic growth and neurotransmission, whereas overexpression reduced the number of stable microtubules. Consistent with this, spastin-deficient zebrafish embryos exhibit a disordered microtubule network (25). However, dramatically impaired outgrowth of motor axons from the spinal cord was also observed in these embryos, associated with aberrant positioning of branchio-motor neuron cell bodies. In contrast, mutation of the *Sp* gene in human or mouse (this study) causes neurodegeneration in adulthood. The severe phenotype observed in zebrafish is likely to be caused by the complete knock-out of *Sp*. In contrast, the majority of HSP patients carry heterozygous mutations, most of them leading to loss of function and, therefore, haploinsufficiency. It is also possible, however, that the difference in CNS motor organization between zebrafish and higher organisms might account for the distinct phenotype of the *Sp* mutation.

Primary cultures of cortical neurons derived from mutant *Sp* embryos exhibit the same focal swellings of neurites associated with abnormal accumulation of organelles, including
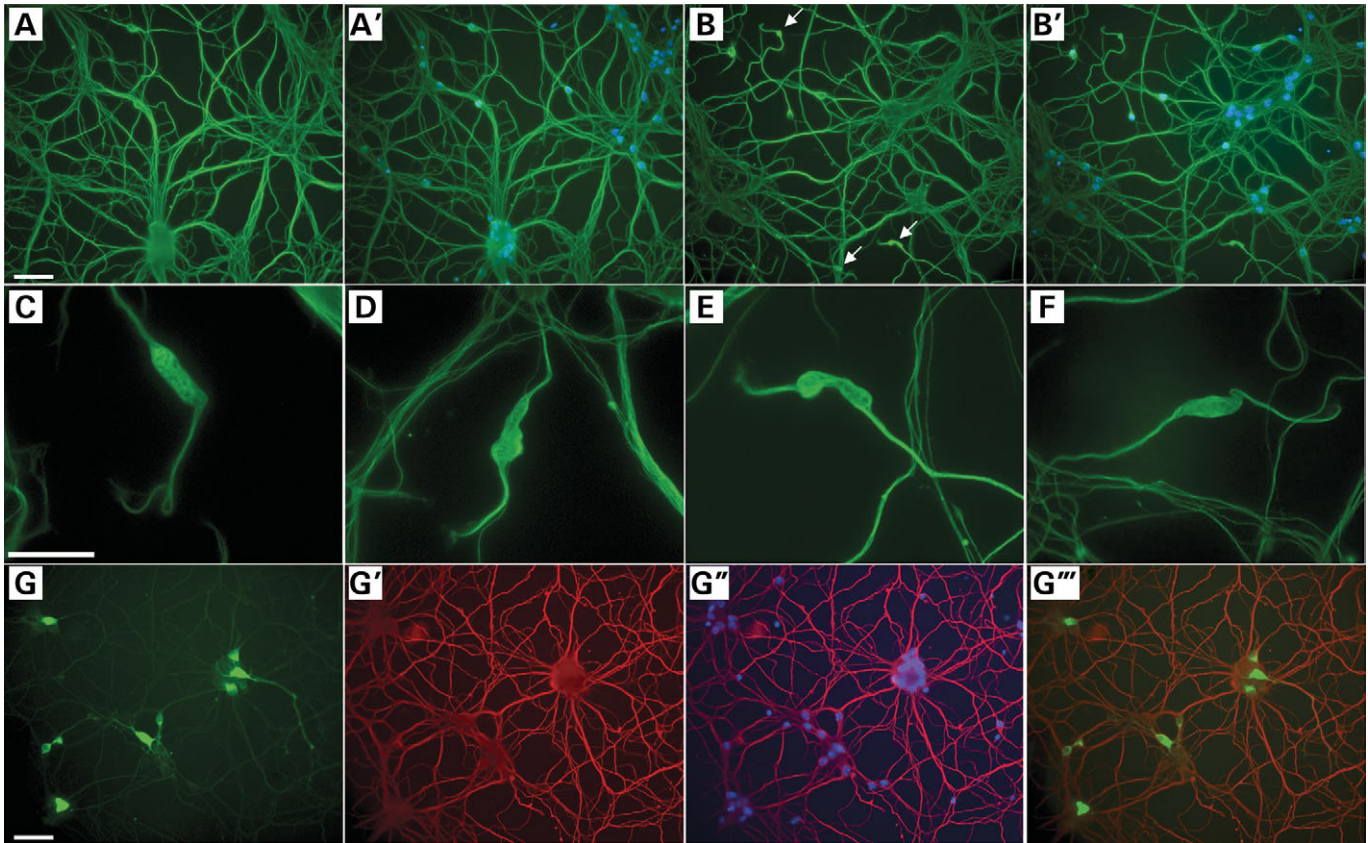
Figure 7. Neurite swellings of cortical neurons derived from mutant embryos. (**A–F**) Primary cultures of cortical neurons derived from wild-type ($Sp^{+/+}$) (A and A′) and mutant 14 d.p.c embryos ($Sp^{\Delta/\Delta}$) (B–F) were immunolabelled with acetylated tubulin antibody (A–F) 6 days after plating. Nuclei were stained with Dapi (A′ and B′). Note the presence of neurite swellings at low (arrows) (B and B′) or high magnification (C–F). (**G–G‴**) Transfection experiment of wild-type cortical neurons with mutant *spastin* fused to GFP (*GFP-Sp*$^{\Delta}$). GFP expression (G), immunolabelling of acetylated tubulin (G′), acetylated tubulin and Dapi (G″) or GFP (G‴). Note the absence of neurite swellings in transfected neurons. Scale bar: (A–B′ and G–G‴) 50 μm; (C–F), 25 μm.

mitochondria and peroxysomes, as those found in the mutant mice. The lack of glial cells in primary cultures of neurons indicates that the neurite defect observed in mutant neurons is a cell autonomous process and does not result from defective glial cells, as previously described in other mouse models of spastic paraplegia, such as PLP-deficient mice (30). In contrast, the early occurrence of neurite swellings in *spastin* mutant cells (from day 4 after plating) compared with the late onset of axonal defects in *spastin* mutant mice *in vivo* could be due to a putative protective effect of the cell environment on axonal maintenance *in vivo*. Survival of mutant cortical neurons was similar to that of controls, demonstrating that the *spastin* mutation does not affect neuron survival, in agreement with *in vivo* data and the human HSP disease phenotype. Interestingly, neurite swellings are associated with an abnormal accumulation of both mitochondria and peroxysomes in the proximal part of swellings, suggesting a focal impairment of retrograde transport of these organelles. The absence of organelle accumulation in other cell compartments both *in vivo* and *in vitro* suggests that this axonal transport defect is restricted to this specialized region of the axon. Further study of axonal transport will help to elucidate whether this defect is restricted to these organelles and represents a primary event leading to progressive neurite swellings.

The most striking feature was the localization of neurite swellings in a specialized region of the axon characterized by the transition between stable and dynamic domains that differ in the composition of post-translationally modified tubulin subunits (28,29). One of these modifications, known as the tyrosination cycle, involves the enzymatic cyclic removal of the C-terminal tyrosine residue of the α-tubulin chain by a (so far uncharacterized) tubulin carboxypeptidase and the re-addition of a tyrosine residue at the same location by tubulin-tyrosine-ligase (31,32). The tyrosination cycle generates two α-tubulin variants, intact tyrosinated tubulin (Tyr-tubulin) and detyrosinated tubulin (Glu-tubulin), which lacks the C-terminal tyrosine of α-tubulin. In cultured cells, Tyr-tubulin is widely distributed in cytoplasmic microtubules, whereas Glu-tubulin is enriched in stable microtubules exhibiting little dynamic behaviour (33–35). Here, we show that the *spastin* mutation results in neurite swellings contiguous with the transition between the stable and dynamic domain of the axon located close to, but distinct from, the growth cone. These results highlight the involvement of spastin in microtubule dynamics and neurite homeostasis in a highly specific region of the axon. Swellings are restricted to this specialized region of axon, and this may explain their low frequency. In addition, the difference in composition and stability
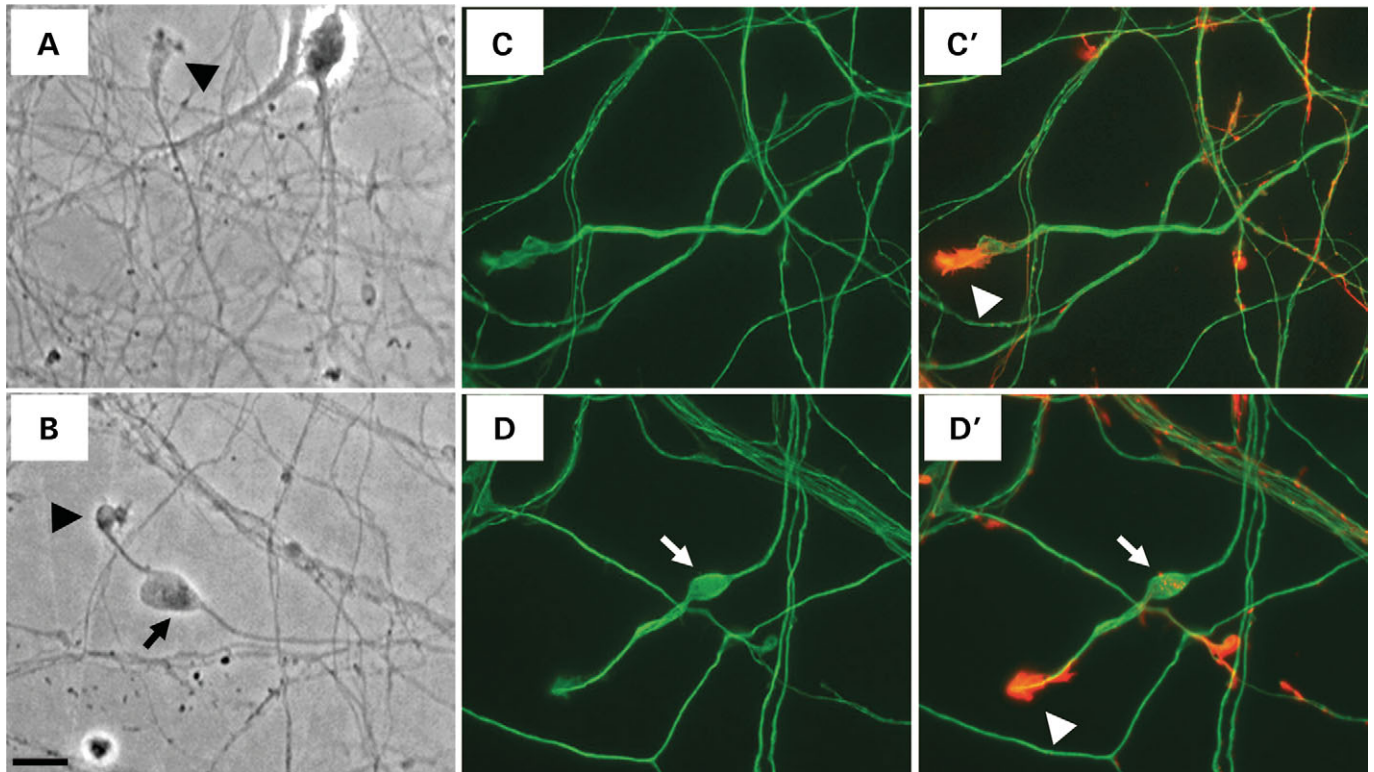
Figure 8. Neurite swellings of mutant cortical neurons are localized closed to the growth cone. Primary cultures of cortical neurons derived from wild-type ($Sp^{+/+}$) (**A**, **C** and **C′**) and mutant 14 d.p.c embryos ($Sp^{\Delta/\Delta}$) (**B**, **D** and **D′**) 6 days after plating. Phase contrast demonstrates both the growth cone (arrowhead) and neurite swelling (arrow) in mutant neurons (B). Note the increased density of neurite swelling content in the proximal part of axon. Immunolabelling of acetylated tubulin (green) (C, C′, D and D′) and actin (phalloidin in red) (C′ and D′) confirms the close proximity of the neurite swelling to the growth cone. Scale bar: 10 μm.

of microtubules in this critical region could provide an explanation for the focal distribution of defects along the length of axons.

These data strongly suggest an important role of spastin in the regulation of microtubule stability. Recently, using purified components, Evans *et al*. (18) have shown that spastin interacts directly with microtubules and is sufficient for microtubule severing. Several mutations, including missense mutations in amino acids that are conserved in the AAA domain and including Walker A and B motifs of the AAA module, disrupt this activity (18). These mutations prevent ATP binding or allow ATP binding but prevent hydrolysis, thereby significantly eliminating ATPase activity. Thus, the AAA domain, deleted in our mutant mice, is involved in ATPase activity which is required for microtubule severing. Microtubule severing occurs in the cell body of the neuron (15), at sites of axonal branch formation (36) and within the growth cones (37). Although the specialized region of the axon in which neurite swellings occur in response to a *spastin* mutation has been previously shown to differ in the composition and stability of its microtubules, little is known about microtubule severing in this region. In addition, an important question is whether spastin acts directly on tubulin composition within this specialized region. Transfection experiments of wild-type *spastin* fused to GFP were performed in the NSC34 neuronal cell line (38), and primary

culture of wild-type cortical neurons revealed the presence of spastin in both cytoplasm and neurites (Online Supplementary Material 5). Spastin was enriched in discrete regions in neurites, in a pattern similar to that described in immortalized neuron cell lines (17). The subcellular localization of spastin in neurites is therefore consistent with a possible direct role of spastin in the transition between stable and labile microtubule domains in the axon. Further studies are clearly required to define the localization and the role of spastin in the regulation of microtubule dynamics in this highly specialized region of the axon and to ascertain the link with axonal transport. During bidirectional transport of molecules or organelles, the net direction of axonal transport is determined by the balance of plus- and minus-end motors. Kinesins are plus-end-directed microtubule motors, whereas dynein is a minus-end-directed microtubule motor (39). In mutant neurons, an abnormal change in microtubule dynamics could lead to a defective interaction of dynein with plus-end microtubules, resulting in a focal defect of retrograde transport.

Interestingly, both *in vivo* and *in vitro* data demonstrate that homozygous mutations resulted in a more severe phenotype than heterozygous mutations, which strongly suggests a haploinsufficiency mechanism underlying spastin-associated HSP. The lack of neurite swellings in wild-type neurons transfected with mutant *spastin* further supports a loss of function, rather than a dominant effect, as the mechanism underlying HSP.
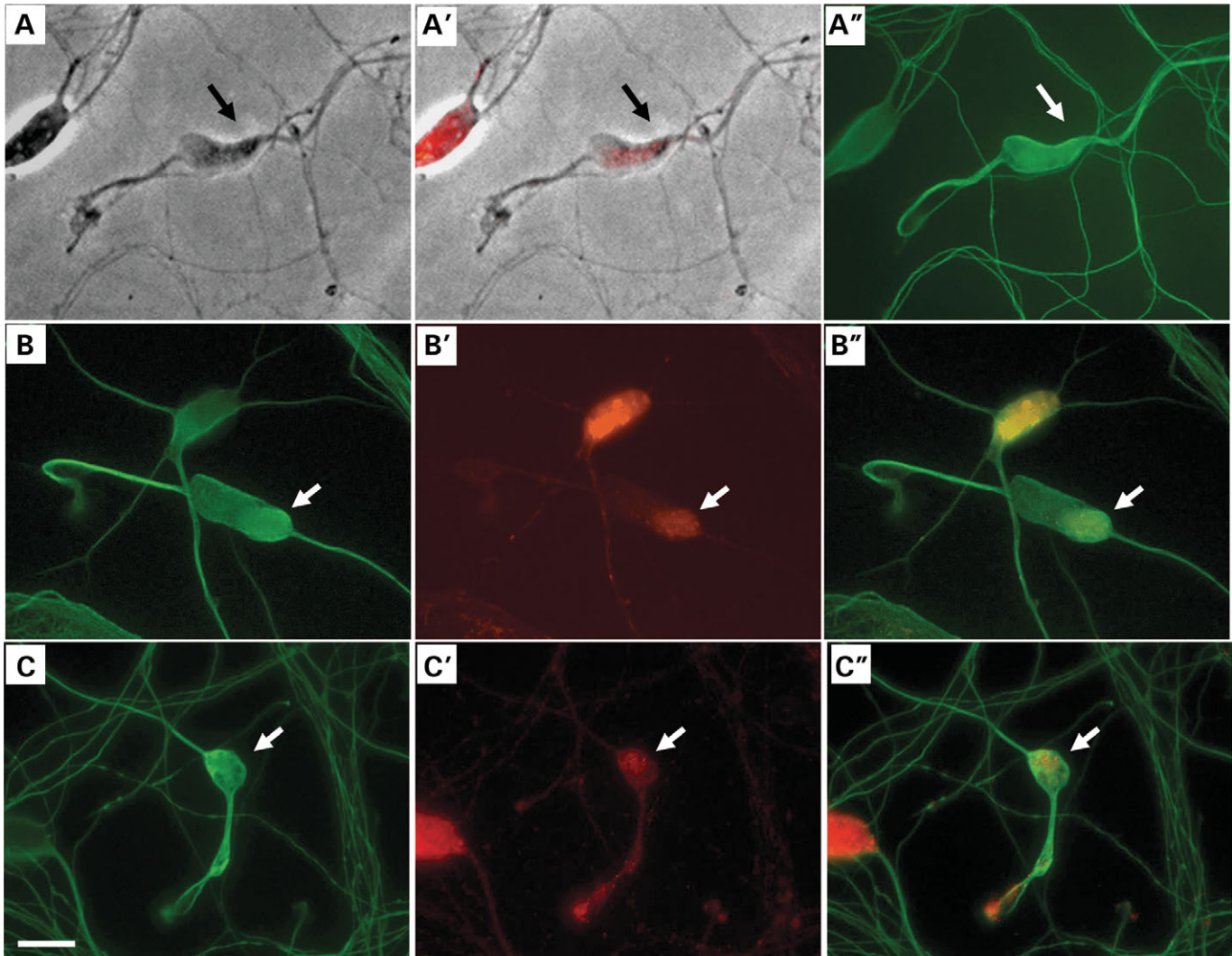
Figure 9. Accumulation of mitochondria and peroxysomes in the proximal region of neurite swellings. Primary cultures of cortical neurons derived from mutant embryos 6 days after plating ($Sp^{\Delta/\Delta}$). Phase contrast (**A** and **A′**), immunolabelling of acetylated tubulin (green) (**A″**, **B**, **B″**, **C** and **C″**), mitotraker (A′, **B′** and B″) and catalase (**C′** and C″) are shown. Note the increased density of neurite swelling (A and A′) associated with the accumulation of mitochondria (arrow) (B′ and B″) and peroxysomes (C′ and C″) in the proximal part of the axonal swelling. (A′, B″ and C″) are merged images. Scale bar: 10 μm.

These results are in agreement with recent *in vitro* data showing that several disease-associated mutations in spastin abolished both ATPase and microtubule-severing activities (18).

In spite of the evidence for their involvement in distinct processes, mutations of *paraplegin*, *PLP*, *KIF5A* or *spastin* (this study) all lead to axonal degeneration and transport defect (30,40,41). These data strongly suggest that axonal transport defect is an important mechanism underlying the pathogenesis of HSP. Axonopathy and alteration of axonal transport have been suggested in various other neurodegenerative disorders including Alzheimer's disease (42). However, here we show that the *spastin* mutation leads to axonal defects and alteration of axonal transport of organelles restricted to a specialized region of the axon close to its tip. This study is the first description of a human neurodegenerative disorder triggering this highly specialized region of the axon, both *in vivo* and *in vitro*. It will be of interest to determine whether the

degenerative process starting from this critical region of the axon is specific to the *spastin* mutation or also occurs in other neurodegenerative disorders. Further study on the composition and the regulation of microtubule dynamics in this region of the axon will be a starting point for the development of therapeutics for HSP.

MATERIAL AND METHODS

Gene targeting and generation of mice

A 10.5 kb mouse genomic BAC-derived DNA fragment containing *spastin* exons 5–7 was cloned into pcDNA 2.1. The LoxP sequences were inserted into introns 4 and 7 in *Sph*1 and *Eco*RV restriction sites, respectively. Two recombinant ES clones (clones C3 and C4) were selected. Mice harbouring the targeted allele were identified by genotype analysis using
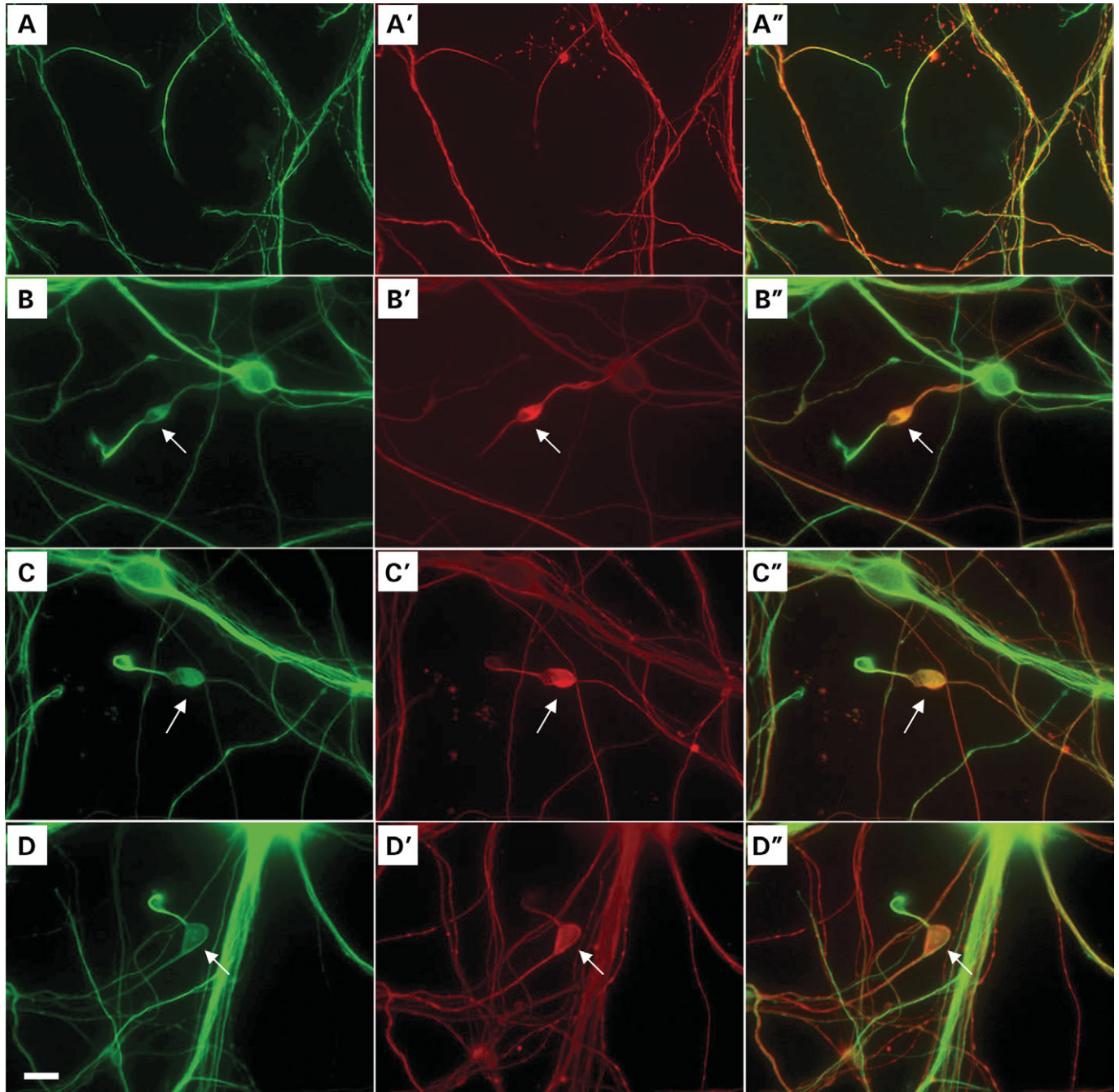
Figure 10. Neurite swellings are located at the transition between stable and labile microtubule domains. Primary culture of cortical neurons derived from control $(Sp^{+/+})$ (**A**–**A″**) and mutant embryos $(Sp^{\Delta/\Delta})$ (**B**–**D″**). Immunolabelling of Tyr-tubulin (A, B, C and D) and Glu-tubulin (A′, B′, C′ and D′). At the tip of axons, Tyr-tubulin is solely expressed, whereas in the other regions of axons, both tubulins are expressed in either control or mutant neurons. In mutant neurons, note that the neurite swellings are always localized proximal to the transition between labile (distal) and stable microtubule regions. Merged images (A″, B″, C″ and D″). Scale bar: 10 μm.

primers *spin7R* (5′-GCCATACAATCTATGGACTTCCA-3′) and *spin7F* (5′-CTACACAGAGAAACCCA GTCTTG-3′) to reveal Sp^+ (190 bp) or Sp^F (340 bp) alleles. The (*CMV-Cre*) transgenic line (26) was used to induce *spastin* deletion. Mice carrying a heterozygous deletion of *spastin* exons 5–7 $(Sp^{\Delta/+})$ in all cell types were generated and intercrossed. The truncated gene was detected by using primers *spin7R*

and *spin4F* (5′-TGACTCCGTCATTG AGACCTGTA-3′, 850 bp). Total RNAs were isolated using Trizol (Invitrogen). cDNAs were amplified by PCR using primers *Slymph* (5′-TGACTAATTTGGTAATCCAG-3′) and *ex12spas* (5′-CCC ATT ACA AGT ACT CTG TC-3′) and sequenced. (Sp^+), $(Sp^{F/+})$, $(Sp^{\Delta/+})$ and $(Sp^{\Delta/\Delta})$ mice were maintained on the same genetic background (C57BL6J). The level of

spastin transcripts was evaluated using the quantity one software (Biorad) in ($Sp^{+/+}$), ($Sp^{F/+}$), ($Sp^{F/F}$), ($Sp^{\Delta/+}$) and ($Sp^{\Delta/\Delta}$) mice (three mice in each group). All animal procedures were performed in accordance with institutional guidelines (agreement B91-228-2 and 3429).

Generation of spastin antibodies and plasmid constructs

Rabbit spastin-specific antibodies were generated against a synthetic peptide located within the deleted region (residues 116–250, Eurogentec, Belgium). NSC-34 cells (38) were transiently transfected with GFP-Sp^{+} or GFP-Sp^{Δ} constructs (see subsequently and Online Supplementary Material 6). Immunoblotting of protein extracts was performed using anti-Sp rabbit antiserum (4828, 1:10 000) or anti-GFP (1:8000, Molecular probes). Spastin constructs were generated by PCR amplification of the *spastin* coding region from the I.M.A.G.E. Consortium Clone 6441742 (43). The resulting fragment was then subcloned in frame into the eukaryotic expression vector pcx-lGN, which contains GFP at the 5' end (GFP-Sp^{+}). The deleted-*spastin* construct (GFP-Sp^{Δ}) composed of exons 1–4 fused to exon 8 was generated by PCR amplification. Sequencing confirmed the integrity of coding regions of both constructs.

Western blot analysis

Immunoblots were performed from total protein extracts of the brain and spinal cord from 12- or 24-month-old control ($Sp^{F/+}$, $n = 3$) and mutant mice ($Sp^{\Delta/\Delta}$, $n = 3$). Immunoblotting was performed using polyclonal antibodies anti-spastin (4828, 1:10 000), kinesin light chain (1:500, Santa Cruz Biotechnology), NF68 (1:20 000, Chemicon) or mouse monoclonal antibodies anti-actin (1:10 000, Sigma), p50 dynactin (1:2000, Transduction Laboratories), p150 glued (1:20 000, Transduction Laboratories), dynein intermediate chain (DIC, 1:2000, Chemicon), α-tubulin (1:5000, Chemicon), phospho-NF200 (1:15 000, Chemicon), anti-NF160 (1:40 000, Chemicon), Tyr-α-tubulin (clone YL1/2, 1:50 000, kindly provided by D. Job), Glu-α-tubulin (1:800 000, kindly provided by D. Job) and γ-enolase (1:20 000, kindly provided by A. Keller). Immunoblot analysis of Tyr-, Glu-tubulins and actin was performed from total protein extracts of primary cultures of cortical neurons from control ($Sp^{+/+}$, $n = 3$) and mutant mice ($Sp^{\Delta/\Delta}$, $n = 3$).

Histological and ultrastructural analyses

Mice were anaesthetized and processed as previously described (44). Semi-thin transverse sections (0.5 μm) were stained with toluidine blue and examined under a Zeiss Axiophot microscope. Ultrathin sections were stained with uranyl acetate and lead citrate and examined with a Tecnai F20 transmission electron microscope (Philips), operating at 200 kV. Axonal surface was assessed from electron micrographs of randomly selected transverse thin sections of lumbar spinal cord using the quantity one software (Biorad). Density of neurons was evaluated on toluidine blue-stained transverse sections of the motor cortex and the anterior horns of the spinal cord.

Primary culture of cortical neurons

Primary cultures of cortical neurons were prepared from 14 d.p.c. embryos. The cortices of embryos were dissected in Mg^{2+}, Ca^{2+}-free HBSS. Tissues were initially dissociated by trypsin, mechanically dissociated by repeated triturations, washed and then spun through a BSA cushion. Cortical neurons were plated on poly-D-ornithine (5 μg/ml) and laminin (2 μg/ml) coated dishes at a density of 9.3×10^4 cells/cm^2 in Neurobasal medium (Invitrogen) plus B27 supplement. Cells were maintained for 6 days at 37°C in 5% CO_2. Cultured cortical neurons were processed for immunofluorescent staining of microtubules (acetylated tubulin, 1:10 000, Sigma), neurofilament (SMI31, 1:500, Chemicon), GFAP (1:100, Sigma), catalase (1:100, Rockland), actin (rhodamine phalloidin, 1:200, Molecular Probes), mitochondria (Mitotraker Orange CM-H2TMRos, 150 nM, Molecular Probes), Tyr- and Glu-tubulins (1:6000 and 1:3000, respectively). Transfection experiments were performed using the Nucleofector apparatus (Amaxa Biosystems) using 1–4 μg of DNA (*pcx-lGN*, GFP-Sp^{+} or GFP-Sp^{Δ}). Neurite outgrowth assessment was performed using a stereological method, as previously described by Ronn *et al.* (45).

Behavioural testing

Spontaneous motor activity. Mice were placed in a cage with infrared beams at two levels in order to detect horizontal and vertical mouse movements. The number of times the mice crossed the infrared beams during a night period of 12 h was recorded. Mice were studied from 3 to 24 months of age.

Footprint analysis. After coating the hind feet with non-toxic ink, mice were allowed to walk through a tunnel (50 cm length, 9 cm wide and 6 cm high) with paper lining the floor. The footprint pattern generated was scored for several parameters as previously described (46). Data were analysed using an unpaired *t*-test.

Evaluation of the CS. CS is an index of the aerobic motor capacity, based on the hyperbolic relationship between speed and time to fatigue in individuals performing exhaustive runs at different speeds. The protocol consisted of a run once a day on a 10.6×30 cm treadmill (LE 8709, Bioseb, Chaville, France) at constant speed leading to exhaustion as previously described (27). This trial was repeated four consecutive days at a different speed. The time the mice were able to run was recorded at each speed and was arbitrarily limited to 40 min or exhaustion as defined by a total number of 20 shocks. The CS was calculated from the slope of the regression line, plotting the distance versus the time to exhaustion for the four runs. In our study, the CS was measured in four homozygous mutant ($Sp^{\Delta/\Delta}$) and three control mice ($Sp^{F/+}$) at 15 and 24 months.

SUPPLEMENTARY MATERIAL

Supplementary Material is available at HMG Online.

Conflict of Interest statement. None declared.

REFERENCES

1. Reid, E. (2003) Science in motion: common molecular pathological themes emerge in the hereditary spastic paraplegias. *J. Med. Genet.*, **40**, 81–86.
2. Soderblom, C. and Blackstone, C. (2005) Traffic accidents: Molecular genetic insights into the pathogenesis of the hereditary spastic paraplegias. *Pharmacol. Ther.*, **109**, 42–56.
3. Hazan, J., Fonknechten, N., Mavel, D., Paternotte, C., Samson, D., Artiguenave, F., Davoine, C.S., Cruaud, C.S., Durr, A., Wincker, P. *et al.* (1999) Spastin, a new AAA protein, is altered in the most frequent form of autosomal dominant spastic paraplegia. *Nat. Genet.*, **23**, 296–303.
4. Fonknechten, N., Mavel, D., Byrne, P., Davoine, C.S., Cruaud, C., Bonsch, D., Samson, D., Coutinho, P., Hutchinson, P., McMonagle, P. *et al.* (2000) Spectrum of SPG4 mutations in autosomal dominant spastic paraplegia. *Hum. Mol. Genet.*, **9**, 637–644.
5. Lindsey, J.C., Lusher, M.E., McDermott, C.J., White, K.D., Reid, E., Rubinsztein, D.C., Bashir, R., Hazan, J., Shaw, P.J. and Bushby, K.M. (2000) Mutation analysis of the spastin gene (SPG4) in patients with hereditary spastic paraparesis. *J. Med. Genet.*, **37**, 759–765.
6. Svenson, I.K., Ashley-Koch, A.E., Gaskell, P.C., Riney, T.J., Cumming, W.J., Kingston, H.M., Hogan, E.L., Boustany, R.M., Vance, J.M., Nance, M.A. *et al.* (2001) Identification and expression analysis of spastin gene mutations in hereditary spastic paraplegia. *Am. J. Hum. Genet.*, **68**, 1077–1085.
7. Patrono, C., Casali, C., Tessa, A., Cricchi, A., Fortini, D., Carrozzo, R., Siciliano, G., Bertini, E. and Santorelli, F.M. (2002) Missense and splice site mutations in SPG4 suggest loss-of-function in dominant spastic paraplegia. *J. Neurol.*, **249**, 200–205.
8. Meijer, I.A., Hand, C.K., Cossette, P., Figlewicz, D.A. and Rouleau, G.A. (2002) Spectrum of SPG4 mutations in a large collection of North American families with hereditary spastic paraplegia. *Arch. Neurol.*, **59**, 281–286.
9. Yip, A.G., Durr, A., Marchuk, D.A., Ashley-Koch, A., Hentati, A., Rubinsztein, D.C. and Reid, E. (2003) Meta-analysis of age at onset in spastin-associated hereditary spastic paraplegia provides no evidence for a correlation with mutational class. *J. Med. Genet.*, **40**, e106.
10. Depienne, C., Tallaksen, C., Lephay, J.Y., Bricka, B., Poea-Guyon, S., Fontaine, B., Labauge, P., Brice, A. and Durr, A. (2006) Spastin mutations are frequent in sporadic spastic paraparesis and their spectrum is different from the one observed in familial cases. *J. Med. Genet.*, **43**, 259–265.
11. Charvin, D., Cifuentes-Diaz, C., Fonknechten, N., Joshi, V., Hazan, J., Melki, J. and Betuing, S. (2003) Mutations of SPG4 are responsible for a loss of function of spastin, an abundant neuronal protein localized in the nucleus. *Hum. Mol. Genet.*, **12**, 71–78.
12. Errico, A., Ballabio, A. and Rugarli, E.I. (2002) Spastin, the protein mutated in autosomal dominant hereditary spastic paraplegia, is involved in microtubule dynamics. *Hum. Mol. Genet.*, **11**, 153–163.
13. Lupas, A.N. and Martin, J. (2002) AAA proteins. *Curr. Opin. Struct. Biol.*, **12**, 746–753.
14. Ahmad, F.J., Yu, W.F., McNally, J. and Baas, P.W. (1999) An essential role for katanin in severing microtubules in the neuron. *J. Cell Biol.*, **145**, 305–315.
15. Karabay, A., Yu, W., Solowska, J.M., Baird, D.H. and Baas, P.W. (2004) Axonal growth is sensitive to the levels of katanin, a protein that severs microtubules. *J. Neurosci.*, **24**, 5778–5788.
16. Nicolai, M., Lasbleiz, C. and Dura, J.M. (2003) Gain-of-function screen identifies a role of the Src64 oncogene in Drosophila mushroom body development. *J. Neurobiol.*, **57**, 291–302.
17. Errico, A., Claudiani, P., D'Addio, M. and Rugarli, E.I. (2004) Spastin interacts with the centrosomal protein NA14, and is enriched in the spindle pole, the midbody and the distal axon. *Hum. Mol. Genet.*, **13**, 2121–2132.
18. Evans, K.J., Gomes, E.R., Reisenweber, S.M., Gundersen, G.G. and Lauring, B.P. (2005) Linking axonal degeneration to microtubule remodeling by Spastin-mediated microtubule severing. *J. Cell Biol.*, **168**, 599–606.
19. Patel, H., Cross, H., Proukakis, C., Hershberger, R., Bork, P., Ciccarelli, F.D., Patton, M.A., McKusick, V.A. and Crosby, A.H. (2002) SPG20 is mutated in Troyer syndrome, an hereditary spastic paraplegia. *Nat. Genet.*, **31**, 347–348.
20. Reid, E., Connell, J., Edwards, T.L., Duley, S., Brown, S.E. and Sanderson, C.M. (2005) The hereditary spastic paraplegia protein spastin interacts with the ESCRT-III complex-associated endosomal protein CHMP1B. *Hum. Mol. Genet.*, **14**, 19–38.
21. Sanderson, C.M., Connell, J.W., Edwards, T.L., Bright, N.A., Duley, S., Thompson, A., Luzio, J.P. and Reid, E. (2006) Spastin and atlastin, two proteins mutated in autosomal-dominant hereditary spastic paraplegia, are binding partners. *Hum. Mol. Genet.*, **15**, 307–318.
22. Mannan, A.U., Boehm, J., Sauter, S.M., Rauber, A., Byrne, P.C., Neesen, J. and Engel, W. (2006) Spastin, the most commonly mutated protein in hereditary spastic paraplegia interacts with Reticulon 1 an endoplasmic reticulum protein.. *Neurogenetics*, **7**, 93–103.
23. Mannan, A.U., Krawen, P., Sauter, S.M., Boehm, J., Chronowska, A., Paulus, W., Neesen, J. and Engel, W. (2006) ZFYVE27 (SPG33), a novel spastin-binding protein, is mutated in hereditary spastic paraplegia. *Am. J. Hum. Genet.*, **79**, 351–357.
24. Trotta, N., Orso, G., Rossetto, M.G., Daga, A. and Broadie, K. (2004) The hereditary spastic paraplegia gene, spastin, regulates microtubule stability to modulate synaptic structure and function. *Curr. Biol.*, **14**, 1135–1147.
25. Wood, J.D., Landers, J.A., Bingley, M., McDermott, C.J., Thomas-McArthur, V., Gleadall, L.J., Shaw, P.J. and Cunliffe, V.T. (2006) The microtubule-severing protein Spastin is essential for axon outgrowth in the zebrafish embryo. *Hum. Mol. Genet.*, **15**, 2763–2771.
26. Dupe, V., Davenne, M., Brocard, J., Dolle, P., Mark, M., Dierich, A., Chambon, P. and Rijli, F.M. (1997) *In vivo* functional analysis of the Hoxa-1 3′ retinoic acid response element (3′RARE). *Development*, **124**, 399–410.
27. Billat, V.L., Mouisel, E., Roblot, N. and Melki, J. (2005) Inter- and intrastrain variation in mouse critical running speed. *J. Appl. Physiol.*, **98**, 1258–1263.
28. Baas, P.W. and Black, M.M. (1990) Individual microtubules in the axon consist of domains that differ in both composition and stability. *J. Cell Biol.*, **111**, 495–509.
29. Brown, A., Li, Y., Slaughter, T. and Black, M.M. (1993) Composite microtubules of the axon: quantitative analysis of tyrosinated and acetylated tubulin along individual axonal microtubules. *J. Cell Sci.*, **104**, 339–352.
30. Griffiths, I., Klugmann, M., Anderson, T., Yool, D., Thomson, C., Schwab, M.H., Schneider, A., Zimmermann, F., McCulloch, M., Nadon, N. *et al.* (1998) Axonal swellings and degeneration in mice lacking the major proteolipid of myelin. *Science*, **280**, 1610–1613.
31. Barra, H.S., Arce, C.A. and Argarana, C.E. (1988) Posttranslational tyrosination/detyrosination of tubulin. *Mol. Neurobiol.*, **2**, 133–153.
32. Ersfeld, K., Wehland, J., Plessmann, U., Dodemont, H., Gerke, V. and Weber, K. (1993) Characterization of the tubulin-tyrosine ligase. *J. Cell Biol.*, **120**, 725–732.
33. Gundersen, G.G., Kalnoski, M.H. and Bulinski, J.C. (1984) Distinct populations of microtubules: tyrosinated and nontyrosinated alpha tubulin are distributed differently *in vivo*. *Cell*, **38**, 779–789.
34. Kreis, T.E. (1987) Microtubules containing detyrosinated tubulin are less dynamic. *EMBO J.*, **6**, 2597–2606.

35. Wehland, J. and Weber, K. (1987) Turnover of the carboxy-terminal tyrosine of alpha-tubulin and means of reaching elevated levels of detyrosination in living cells. *J. Cell Sci.*, **88**, 185–203.

36. Yu, W., Ahmad, F.J. and Baas, P.W. (1994) Microtubule fragmentation and partitioning in the axon during collateral branch formation. *J. Neurosci.*, **14**, 5872–5884.

37. Dent, E.W., Callaway, J.L., Szebenyi, G., Baas, P.W. and Kalil, K. (1999) Reorganization and movement of microtubules in axonal growth cones and developing interstitial branches. *J. Neurosci.*, **19**, 8894–8908.

38. Cashman, N.R., Durham, H.D., Blusztajn, J.K., Oda, K., Tabira, T., Shaw, I.T., Dahrouge, S. and Antel, J.P. (1992) Neuroblastoma x spinal cord (NSC) hybrid cell lines resemble developing motor neurons. *Dev. Dyn.*, **194**, 209–221.

39. Welte, M.A. (2004) Bidirectional transport along microtubules. *Curr. Biol.*, **14**, R525–R537.

40. Ferreirinha, F., Quattrini, A., Pirozzi, M., Valsecchi, V., Dina, G., Broccoli, V., Auricchio, A., Piemonte, F., Tozzi, G., Gaeta, L. *et al.* (2004) Axonal degeneration in paraplegin-deficient mice is associated with abnormal mitochondria and impairment of axonal transport. *J. Clin. Invest.*, **113**, 231–242.

41. Xia, C.H., Roberts, E.A., Her, L.S., Liu, X., Williams, D.S., Cleveland, D.W. and Goldstein, L.S. (2003) Abnormal neurofilament

42. Stokin, G.B., Lillo, C., Falzone, T.L., Brusch, R.G., Rockenstein, E., Mount, S.L., Raman, R., Davies, P., Masliah, E., Williams, D.S. *et al.* (2005) Axonopathy and transport deficits early in the pathogenesis of Alzheimer's disease. *Science*, **307**, 1282–1288.

43. Lennon, G., Auffray, C., Polymeropoulos, M. and Soares, M.B. (1996) The I.M.A.G.E. Consortium: an integrated molecular analysis of genomes and their expression. *Genomics*, **33**, 151–152.

44. Frugier, T., Tiziano, F.D., Cifuentes-Diaz, C., Miniou, P., Roblot, N., Dierich, A., Le Meur, M. and Melki, J. (2000) Nuclear targeting defect of SMN lacking the C-terminus in a mouse model of spinal muscular atrophy. *Hum. Mol. Genet.*, **9**, 849–858.

45. Ronn, L.C., Ralets, I., Hartz, B.P., Bech, M., Berezin, A., Berezin, V., Moller, A. and Bock, E. (2000) A simple procedure for quantification of neurite outgrowth based on stereological principles. *J. Neurosci. Meth.*, **100**, 25–32.

46. Simon, D., Seznec, H., Gansmuller, A., Carelle, N., Weber, P., Metzger, D., Rustin, P., Koenig, M. and Puccio, H. (2004) Friedreich ataxia mouse models with progressive cerebellar and sensory ataxia reveal autophagic neurodegeneration in dorsal root ganglia. *J. Neurosci.*, **24**, 1987–1995.

transport caused by targeted disruption of neuronal kinesin heavy chain KIF5A. *J. Cell Biol.*, **161**, 55–66.